A&A manuscript no.
(will be inserted by hand later)

Your thesaurus codes are:
01 (02.01.2; 02.13.3; 02.23.1; 11.09.1; 11.14.1)

ASTRONOMY
AND
ASTROPHYSICS
17.10.1996

Warping modes in the maser disc of NGC 4258

A. T. Okazaki[1,2]

[1] Astronomical Institute 'Anton Pannekoek', University of Amsterdam, Kruislaan 403, 1098 SJ Amsterdam, The Netherlands
[2] College of General Education, Hokkai-Gakuen University, Toyohira-ku, Sapporo 062, Japan (okazaki@elsa.hokkai-s-u.ac.jp)

Received / Accepted

Abstract. We examine the characteristics of warping modes in the maser disc at the centre of NGC 4258. We find that the velocity field associated with the modes is approximately vertical and that its amplitude decreases with radius. This characteristic accounts for the observed position and velocity distribution of the high-velocity maser features of NGC 4258. We also find that the position-velocity diagram calculated for a disc with a warping perturbation pattern is consistent with the observed redward offset of the low-velocity maser features, if the maser emission arises from the upper-half part of the disc.

Key words: Accretion, accretion disks – Galaxies: individual: NGC 4258 – Galaxies: nuclei – Masers – Waves

1. Introduction

Recent discovery of water mega- and giga-masers in circumnuclear regions of some active galactic nuclei has opened a new way to probe the innermost parsec of the nuclei. The water megamaser sources at the centre of NGC 4258 provide compelling evidence for the presence of a central supermassive black hole (Miyoshi et al. 1995). The position and velocity distribution of these maser sources are fitted well with a warped Keplerian disc model (Miyoshi et al. 1995). From measurements of drift velocities of these sources (Haschik et al. 1994; Greenhill et al. 1995a; Greenhill et al. 1995b; Nakai et al. 1995), with the assumption of Keplerian circular motion, the distance of this galaxy becomes 6.5 ± 0.3 Mpc (Nakai et al. 1995). The mass of the central black hole and the inner and outer radii of the maser emission region are then $3.6 \times 10^7\, M_\odot$, 0.12pc, and 0.26pc, respectively (Nakai et al. 1995). Similar values are derived by Miyoshi et al. (1995). The maser disc is so thin that the upper limit of the disc thickness is 3×10^{-4}pc (Moran et al. 1995).

It is known, however, that near-Keplerian discs can be perturbed by global $m = 1$ oscillations (e.g., Kato 1983). If $m = 1$ modes exist in maser discs, the velocity field should more or less deviate from Keplerian. Hence, in general, these modes can affect the estimate of the distance to galaxies as well as of the masses of central black holes. It is, therefore, important to study the characteristics of $m = 1$ modes in maser discs and their effect on the disc kinematics.

In this paper, we focus our attention on warping modes, i.e., $m = 1$ modes with a density perturbation antisymmetric with respect to the equatorial plane, considering the observed shape of the maser disc of NGC 4258. We show that the characteristics of warping modes are consistent with the observed spatial and velocity distribution of maser sources. We also show how the modes affect the line-of-sight velocities of the low-velocity maser features.

Send offprint requests to: A. T. Okazaki at Sapporo address

2. Disc model and the perturbation equation

We take a non-self-gravitating, axisymmetric disc as an unperturbed equilibrium disc. It rotates around a black hole of mass $M_{\rm BH} = 3.6 \times 10^7\, M_\odot$, of which the Schwarzschild radius $r_g = 3.4 \times 10^{-6}\,$pc. To simulate the weak general relativistic effect, we use the pseudo-Newtonian potential (Paczyński & Wiita 1980). We assume that the geometrically-thin maser disc is in hydrostatic equilibrium in the vertical direction, and has an inner radius, $r_{\rm in}$, and an outer radius, $r_{\rm out}$. We neglect radial advective motions and viscous effects. We use cylindrical coordinates (r, ϕ, z); the z-axis is normal to the disc midplane and is not the vertical axis of the galaxy.

We assume that the gas obeys a polytropic relation with index γ. The unperturbed density distribution is then given by

$$\rho_0(r,z) = \rho_{00}(r) \left[1 - \left(\frac{z}{H}\right)^2\right]^{1/(\gamma-1)}, \qquad (1)$$

where ρ_{00} is the unperturbed density in the equatorial plane, and H the half-thickness of the disc given by $H \sim r^{3/2}\rho_{00}^{(\gamma-1)/2}$. In our model, we are free to specify

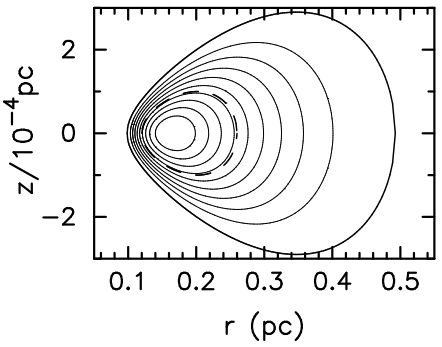

Fig. 1. Density distribution in the unperturbed disc. The dashed line denotes the maser emission region, in which $\rho_0(r,z) \geq \rho_{00}(r_1)$. The contours are separated by 0.1

a functional form of ρ_{00}. For simplicity, we adopt a toy model for ρ_{00},

$$\rho_{00}(r) = \left[\frac{2rr_0 - r_0^2 - Cr^2}{r^2(1-C)}\right]^{1/(\gamma-1)}, \qquad (2)$$

where r_0 is the radius at which the density reaches its maximum [$\rho_{00}(r_0) = 1$], and C a constant defined by $C = 4r_{\rm in}r_{\rm out}/(r_{\rm in}+r_{\rm out})^2$. This density distribution was used by Miyama et al. (1994) to study the stability of circumstellar discs.

Since global features of the eigenmodes are not sensitive to the values of γ, C, and r_0, we adopt a particular density distribution such that $\gamma = 5/3$, $\rho_{00}(r_1) = \rho_{00}(r_2)$, and $r_{\rm out}/r_{\rm in} = 5$. Here, $r_1(= 0.12{\rm pc})$ and $r_2(= 0.26{\rm pc})$ are, respectively, the inner and outer radii of the region from which the maser emission arises. For this particular choice of parameters, $r_0 = 0.164{\rm pc}$, $r_{\rm in} = 0.0995{\rm pc}$, and $r_{\rm out} = 0.493{\rm pc}$. We normalize H such that the maximum half-thickness of the region in which $\rho_0(r,z) \geq \rho_{00}(r_1)$ becomes 10^{-4}pc (hereafter, we refer to this region as the maser emission region). Figure 1 shows the density distribution in the unperturbed disc by contours. In Fig. 1, the dashed line denotes the maser emission region.

We consider a linear, adiabatic $m = 1$ perturbation superposed on the unperturbed disc. The perturbation varies as $\exp[i(\omega t - \phi)]$, where ω is the frequency of the perturbation. After some manipulations, we finally have the following equation describing the linear, adiabatic $m = 1$ perturbation:

$$\frac{\partial^2 h_1}{\partial r^2} - \frac{\partial}{\partial r}\ln\frac{|(\omega-\Omega)^2-\kappa^2|}{\rho_0 r}\frac{\partial h_1}{\partial r} + \left[\frac{(\omega-\Omega)^2-\kappa^2}{c_0^2}\right.$$
$$\left.\frac{2\Omega}{r(\omega-\Omega)}\frac{\partial}{\partial r}\ln\frac{|(\omega-\Omega)^2-\kappa^2|}{\rho_0\Omega} - \frac{1}{r^2}\right] h_1$$
$$+\frac{(\omega-\Omega)^2-\kappa^2}{(\omega-\Omega)^2}\frac{1}{\rho_0}\frac{\partial}{\partial z}\left(\rho_0\frac{\partial h_1}{\partial z}\right) = 0, \qquad (3)$$

where h_1 is the enthalpy perturbation defined by $h_1 = p_1/\rho_0$, p_1 the Eulerian perturbation of the pressure, c_0 the sound speed in the unperturbed disc, and Ω and κ the angular frequency of disc rotation and the epicyclic frequency, respectively.

As the boundary conditions for Eq. (3), we require that the Lagrangian perturbation to the pressure vanishes on the disc surface and $h_1 = 0$ in the equatorial plane. The latter condition is for warping modes. We solve Eq. (3) in the $(\ln r, z/H)$-plane with 101 grid points in the radial direction and 51 grid points in the vertical direction. To avoid singularities, we pose the inner and outer boundaries of the computational domain at $r = (1+\delta)r_{\rm in}$ and $r = (1-\delta)r_{\rm out}$ with $\delta = 10^{-6}$, respectively. We have verified that the value of δ does not affect the global features of the eigenmodes as long as $\delta \ll 1$.

3. Characteristics of warping modes in the maser disc of NGC 4258

Figure 2 shows the structure of the fundamental warping mode: (a) the (r,ϕ)-distribution of the perturbations averaged vertically and (b) the (r,z)-distribution of the perturbations. For the sake of convenience, in Fig. 2(a), we averaged h_1 over $0 \leq z \leq H$ and velocity vectors over $0 \leq z \leq H_{\rm maser}$, where $H_{\rm maser}$ is the half-thickness of the maser emission region shown in Fig. 1. Note that the horizontal velocities as well as h_1 are reversed in the lower half of the disc. For the purpose of comparison between the numerical results and the observations, we draw Fig. 2 such that the disc rotates clockwise. In Fig. 2(b), we superposed the poloidal velocity vectors on the enthalpy perturbation, h_1, despite that the former phase lags behind the latter phase by $\pi/2$. The period of the mode is $\sim 9 \cdot 10^7$ yr, which is about 10^5 times longer than the rotation period at $r = r_1$.

Figure 2 shows several basic features of the fundamental warping mode. Firstly, h_1 and the horizontal component of the perturbed velocity are approximately proportional to the vertical coordinate z/H, whereas the vertical component of the perturbed velocity is approximately constant in the z-direction. Secondly, the velocity vector associated with the warping mode is approximately vertical. The ratio of the horizontal velocity component to the vertical component is roughly $0.1 \cdot z/H$. Thirdly, the amplitudes of h_1 and the vertical velocity component decrease with radius. Note that the first and the third features are consistent with the observed spatial distribution of high-velocity maser components of NGC 4258 [compare Fig. 2 with Fig. 2 of Miyoshi et al. (1995)]. Note also that the second feature is in agreement with the observed near-Keplerian velocity distribution of maser sources of NGC 4258.

Observationally, the line-of-sight velocity distribution of high-velocity maser components are fitted with a Keplerian disc model with such a high accuracy that the velocity residuals are less than a few $\rm km\,s^{-1}$ (Greenhill et al. 1995b). However, the line-of-sight velocity distribution

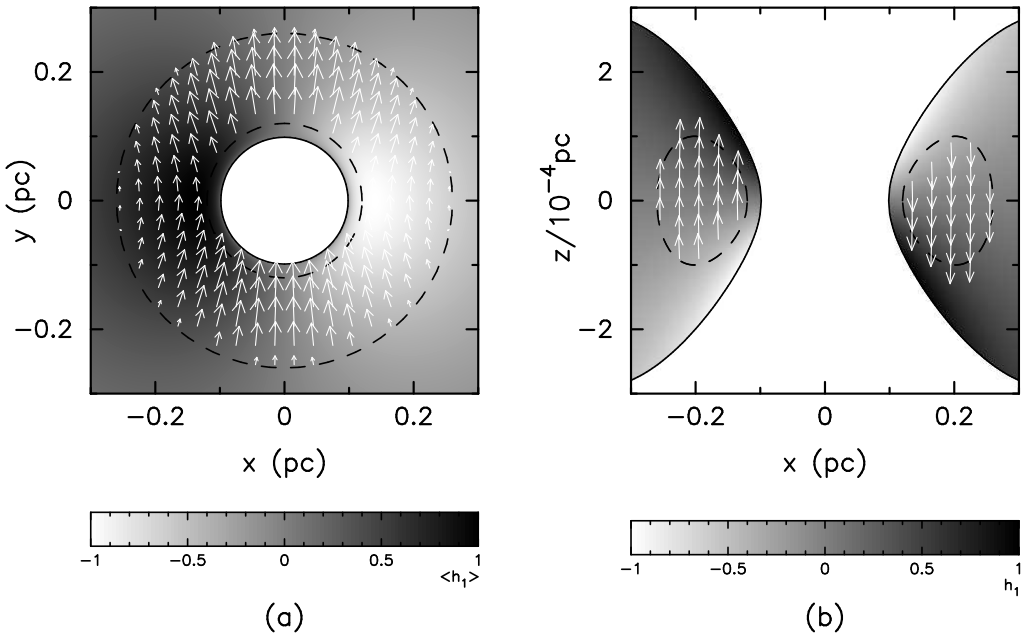

Fig. 2. Structure of the fundamental warping mode. **a** The (r, ϕ)-distribution of the perturbations averaged vertically over the upper half of the disc; the distribution is reversed in the lower half. **b** The (r, z)-distribution of the perturbations. A gray-scale representation denotes h_1. Arrows superposed on the gray-scale plot are the perturbed velocity vectors in the maser emission region (surrounded by dashed lines)

of low-velocity components significantly deviates from the Keplerian curve of the high-velocity components. It is offset redward by $\sim 15 \mathrm{km\,s^{-1}}$ (Nakai et al. 1995). In addition, the slope for low-velocity components with $V_{\rm rel} < 0$ (hereafter, blueshifted low-velocity features) is slightly flatter than that with $V_{\rm rel} > 0$ (hereafter, redshifted low-velocity features), where $V_{\rm rel}$ is the line-of-sight velocity relative to the systemic velocity [see Fig. 19(b) of Nakai et al. (1995)]. This, together with the fact that the drift velocity of low-velocity components is larger ($10.2 \mathrm{km\,s^{-1}}$) at $V_{\rm rel} > 0$ than that ($8.6 \mathrm{km\,s^{-1}}$) at $V_{\rm rel} < 0$, suggests that blueshifted low-velocity features lie at ~ 1.1 times the radii of the redshifted features (Greenhill et al. 1995b; Nakai et al. 1995).

It is obvious that any warped disc model fails if only the vertical component of the perturbed velocity is taken into account. The vertical velocity component consistent with the spatial distribution of the high-velocity maser features of NGC 4258 shifts the line-of-sight velocity of low-velocity features blueward. In order to explain the observed redward-offset, the inward velocity component has to be included. One possible way to include the inward velocity component in our model is to assume that maser features arise only from the upper-half ($z > 0$) part of the disc, which is closer to the line-of-sight through the central pumping source than the lower-half part.

Based on this assumption, we calculate the line-of-sight velocity distribution of maser features in the disc perturbed by the warping mode. For this purpose, we assume the nonlinear perturbation pattern similar to the linear mode shown in Fig. 2. We use the velocity field averaged vertically over $0 \le z \le H_{\rm maser}$. We normalize the amplitude of the perturbation such that the vertical component of the perturbed velocity at $r = r_1$ is 10% of the Keplerian velocity. We take into account the redshift of maser features from the unperturbed disc, which amounts to $3cr_g/4r \simeq 6.5(r/r_1)^{-1} \mathrm{km\,s^{-1}}$, where c is the speed of light [see, e.g., Eq. (A9) of Okazaki et al. (1987)].

Figure 3 shows the model position-velocity diagram. The thick solid lines denote the line-of-sight velocity distribution of maser sources which lie along the x-axis (high-velocity components). Two thin solid lines are for maser sources lying along the radii $r = 0.124$pc and $r = 0.135$pc. These radii correspond to the observed drift velocities of blue- and red-shifted low-velocity features, respectively.

From Fig. 3, we immediately observe the following characteristics of the model diagram:

1. High-velocity maser features do not follow the exact Keplerian distribution. Because of the contribution of the azimuthal component of the perturbed velocity, high-velocity features are shifted redward by an amount somewhat larger than that $[6.5(r/r_1)^{-1} \mathrm{km\,s^{-1}}]$ expected for the unperturbed disc.
2. Low-velocity maser features are offset redward because of the contribution of the radial component of the perturbed velocity. As has pointed out by other authors

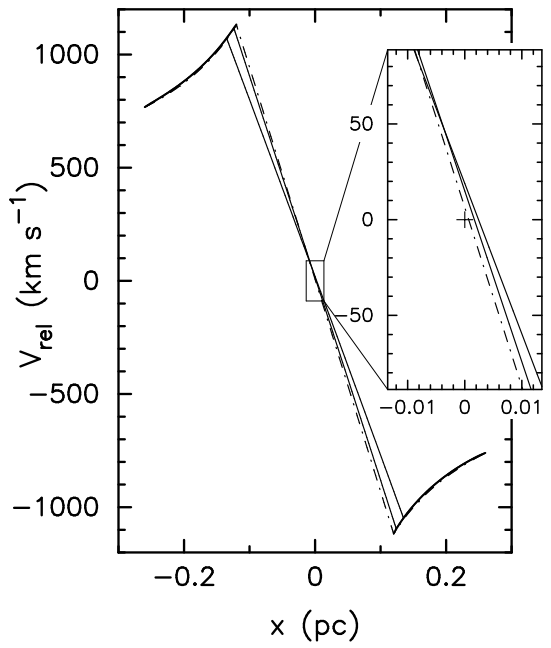

Fig. 3. Position-velocity diagram for the disc perturbed by the fundamental warping mode. The inset is an enlargement of the low-velocity maser features. The inclination angle of the disc is 82°. The thick solid lines denote the line-of-sight velocity distribution of maser sources which lie along the x-axis (high-velocity components). Two thin solid lines are for maser sources lying along $r = 0.124$pc and $r = 0.135$pc, which correspond to the observed drift velocities of blue- and red-shifted low-velocity features, respectively. For comparison purpose, we present the line-of-sight velocity distribution for sources lying along $r = r_1$ in the unperturbed disc (dash-dotted line). The cross in the inset indicates the origin of the diagram

(Greenhill et al. 1995b; Nakai et al. 1995), the difference in radii from which maser emission arises results in a difference in slopes.

Finally, we stress that the warping modes can be excited by several mechanisms. In this paper, we have neglected the effects of viscosity, disc self-gravity, and radiation-pressure force, and, consequently, have treated neutral modes. The viscous force can make $m = 1$ modes overstable in accretion discs (Kato 1989). The disc self-gravity can also excite $m = 1$ modes through the interaction between long waves (e.g., Adams et al. 1989). Moreover, the radiation-driven warping of discs can occur far from central radiation sources (Pringle 1996; Begelman 1996). It is highly desirable to study if these mechanisms work for the particular case of NGC 4258.

4. Conclusions

As a model for the warped maser disc of NGC 4258, we have considered $m = 1$ modes in which the density perturbation is antisymmetric with respect to the equatorial plane. Solving a linear eigenvalue problem in the (r,z)-plane, we have found that the velocity field of the mode is dominated by the vertical component whose amplitude decreases with radius. This characteristic agrees well with the observed spatial- and velocity-distribution of the high-velocity maser features of NGC 4258.

Moreover, we have calculated the position-velocity diagram for the disc with a nonlinear perturbation pattern similar to the linear warping mode. We have found that the model diagram reproduces the observed redward offset of the low-velocity maser features, if the maser emission arises only from the upper-half ($z > 0$) part of the disc. We have also found that the high-velocity maser features should be shifted redward by an amount somewhat larger than that $[6.5(r/r_1)^{-1}\mathrm{km\,s^{-1}}]$ expected for the unperturbed disc.

In our formulation of the eigenvalue problem for warping modes, we have adopted several assumptions for simplicity. The next step should be to formulate the problem with a more realistic disc model in which effects of viscosity, disc self-gravity, and radiation pressure force are taken into account.

Acknowledgements. The author thanks H.F. Henrichs for careful reading of the manuscript. The author also thanks the Astronomical Institute 'Anton Pannekoek' for their warm hospitality. This work was partially supported by a grant from Hokkai-Gakuen Educational Foundation.

References

Adams, F.C., Ruden, S.P., Shu, F.H. 1989, ApJ 347, 959
Begelman, M.C., 1996, In: Wickramasinghe, D., Ferrario, L., Bicknell, G. (eds.) Proc. IAU Colloq 163, Accretion Phenomena and Related Outflows, in press
Greenhill, L.J., Jiang, D.R., Moran, J.M., et al., 1995a, ApJ 440, 619
Greenhill, L.J., Henkel, C., Becker, R., Wilson, T.L., Wouterloot, J.G.A., 1995b, A&A 304, 21
Haschik, A.D., Baan, W.A., Peng, E.W., 1994, ApJ 437, L35
Kato, S., 1983, PASJ 35, 249
Kato, S., 1989, PASJ 41, 745
Miyama, S.M., Nakamoto, T., Kikuchi, N., et al., 1994, In: Franco, J. (ed.) Numerical Simulations in Astrophysics. Cambridge University Press, in press
Miyoshi, M., Moran, J., Herrnstein, J., et al., 1995, Nat 373, 127
Moran, J., Greenhill, L., Herrnstein, J., et al., 1995, In: Quasars and AGN; High Resolution Imaging, in press
Nakai, N., Inoue, M., Miyazawa, K., Miyoshi, M., Hall, P., 1995, PASJ 47, 771
Okazaki, A.T., Kato, S., Fukue, J., 1987, PASJ 39, 457
Paczyński, B, Wiita, P.J., 1980, A&A 88, 23
Pringle, J.E., 1996, MNRAS 281, 357

This article was processed by the author using Springer-Verlag LaTeX A&A style file *L-AA* version 3.